Visual acuity in the archerfish: Behavior, anatomy, and neurophysiology

Avi Ben-Simon
Department of Life Sciences and Zlotowski Center for Neuroscience, Ben-Gurion University of the Negev, Beer-Sheva, Israel

Ohad Ben-Shahar
Department of Computer Science and Zlotowski Center for Neuroscience, Ben-Gurion University of the Negev, Beer-Sheva, Israel

Genadiy Vasserman
Department of Life Sciences and Zlotowski Center for Neuroscience, Ben-Gurion University of the Negev, Beer-Sheva, Israel

Mor Ben-Tov
Department of Life Sciences and Zlotowski Center for Neuroscience, Ben-Gurion University of the Negev, Beer-Sheva, Israel

Ronen Segev
Department of Life Sciences and Zlotowski Center for Neuroscience, Ben-Gurion University of the Negev, Beer-Sheva, Israel

Archerfish are known for their remarkable behavior of shooting water jets at prey hanging on vegetation above water. Motivated by the fish's capacity to knock down small prey as high as two meters above water level, we studied the role of the retina in facilitating their excellent visual acuity. First, we show behaviorally that archerfish (*Toxotes jaculatrix*) can detect visual structures with a minimum angle of resolution in the range of 0.075°–0.15°. Then, combining eye movement measurements with a ray tracing method, we show that the image of a target on the retina coincides with the area centralis at the ventro-temporal retina. Moving down to retinal neural circuits, we then examine the ratio by which retinal ganglion cells multiplex visual information from the photoreceptors. Measuring the anatomical densities of both cell types in the area centralis, we found photoreceptor spacing to be 5.8 μm, which supports a minimum angle of resolution as low as 0.073°. Similarly, the average spacing of the ganglion cells was 5.7 μm. Based on electrophysiological measurements we found the smallest receptive fields of ganglion cells in that area to be in the range of 8–16 μm, which translates to an angular width of 0.1°–0.2°. These findings indicate that retinal ganglion cells in the area centralis stream information to the brain at a comparable resolution with which it is sampled by the photoreceptors. Thus, the archerfish can be used as an animal model for studying how visual details are streamed to the brain by retinal output.

Keywords: visual acuity, eye movements, electrophysiology, archerfish, area centralis

Citation: Ben-Simon, A., Ben-Shahar, O., Vasserman, G., Ben-Tov, M., & Segev, R. (2012). Visual acuity in the archerfish: Behavior, anatomy, and neurophysiology. *Journal of Vision*, *12*(12):18, 1–19, http://www.journalofvision.org/content/12/12/18, doi:10.1167/12.12.18.

Introduction

From detecting a potential predator from far away to identifying the animal's own prey, visual acuity is critical in performing numerous visual tasks. As part of an information processing system, visual acuity is subjected to three internal limiting factors during the flow of visual information from the stimulus to the animal's brain (Land & Nilsson, 2012). First, visual acuity is bounded by the optical quality of the eye, namely, by the maximal sharpness of the image as it is projected on the photoreceptor layer. The second component is the photoreceptor spacing, which determines the sampling frequency of the image at the input of the nervous system (Hirsch & Curcio, 1989). And third, after retinal preprocessing, the image is sent to the brain by the retinal ganglion cells, the only cells that

project axons to the brain (Ikeda, 1979; Rodieck, 1998). Retinal ganglion cells resample the visual information to be processed by higher parts of the visual system, a process that further bounds the best visual acuity the organism can possess.

Evidently, maintaining an eye that imposes no practical limits in all of the above incurs a cost that no organism could sustain during evolution. Hence, the evolutionary process has made various compromises to optimize visual acuity for the available resource. Best known is the emergence of a retinal region specialized for high visual acuity—the *area centralis* (Kolb, 2003; Rodieck, 1998). This region is usually characterized with a high concentric increase of cones and ganglion cells, which reduce two of the three limiting factors mentioned above in a *local* fashion. Typically the area centralis possesses no rods and each ganglion cell receives signal from one to a few cone photoreceptors. Effectively, this permits a representation of the visual information that is constrained mainly by the spacing between the centers of adjacent cone cells. To compensate for this "high-end" apparatus, *peripheral* vision pays the price of having a smaller photoreceptor sampling rate and ganglion cells that receive signals from many cones and rods. It is no surprise then that visual acuity in peripheral vision of such animals is dominated by the large spacing between the centers of receptive fields (RFs) of adjacent ganglion cells. This prevailing architecture requires the ability to change the information projected onto the area centralis. Indeed, such a solution is made possible in most animals via eye and head movements (Land, 1999).

Seemingly consistent with the above architecture, archerfish were recently reported to possess an area centralis on the ventro-temporal retina that may facilitate high visual acuity, which could be used by the fish to shoot accurately at prey above the water (Temple, Hart, Marshall, & Collin, 2010). Moreover, Temple et al. (2010) found two other areas on the retina with high cone density, but only in the ventro-temporal retina was the ganglion cell density the highest (50,000 cells/mm^2) and was a convergence of cone and ganglion cells found. From here onward we will refer to the area on the ventro-temporal retina as the area centralis. The radius of this area was found to be ~0.6 mm (Temple et al., 2010) that translates to an angle of 6° for an eye radius of 4.5 mm (Luling, 1958). Since this animal is used today for studying many aspects of visual processing (Mokeichev, Segev, & Ben-Shahar, 2010; Rossel, Corlija, & Schuster, 2002; Schlegel & Schuster, 2008; Schuster, Rossel, Schmidtmann, Jäger, & Poralla, 2004; Segev, Schneidman, Goodhouse, & Berry, 2007; Timmermans, 2000, 2001; Vasserman, Shamir, Ben Simon, & Segev, 2010; Wohl & Schuster, 2006, 2007), we set out to study the different aspects affecting visual acuity in the archerfish. Our motivation was to characterize visual acuity in this increasingly important model system in order to facilitate further research on the foundation of vision. To do so, this paper presents a combined study involving behavior, anatomy, and electrophysiology to obtain complementary evidence on the role of the archerfish area centralis in acquiring high acuity visual information.

First we show the behavioral limits of visual acuity in the archerfish (*Toxotes jaculatrix*) by determining their minimum angle of resolution. In this part of the study we were inspired by similar exploration in human vision: human subjects with intact vision can identify a stroke of a letter that subtends an angle as small as 1 minute of arc (Rodieck, 1998). This angle translates to an arc distance of ~4 μm for a normal adult eye of 25–30 mm in diameter, which is comparable with the distance between the centers of two adjacent cone photoreceptors in the fovea, i.e., ~2.3 μm. Thus, the limiting factor on the human visual acuity in the center of vision, after the nervous system has sampled the image, is the spacing between the centers of foveal cone photoreceptors (Rodieck, 1998).

By combining the measurement of fish eye movements with intraocular ray tracing (Ben-Simon, Ben-Shahar, & Segev, 2009), we were then able to show that the archerfish does indeed use the anatomically reported area centralis (Temple et al., 2010) to acquire visual information in high resolution. More specifically, we showed how the visual stimulus we used was projected to the area centralis rather than to any other part of the retina. Furthermore, using anatomical measurements, we showed that the fish area centralis has comparable densities of photoreceptors and ganglion cells, which suggest that its retinal ganglion cells do not represent an information bottleneck in this area. To obtain the final functional support for this possibility, we measured ganglion cell RF sizes in both the area centralis and peripheral retina. The results confirm that in the area centralis, ganglion cells have an RF area of two to eight photoreceptors, small enough to avoid the limiting factor associated with the resampling of the visual information by the ganglion cell layer.

Results

Behavioral exploration of visual acuity in archerfish

We tested visual acuity in archerfish (from here on we will refer to the archerfish species *Toxotes jaculatrix* as archerfish) through experiments that were set to examine the minimum angle of resolvable resolution.

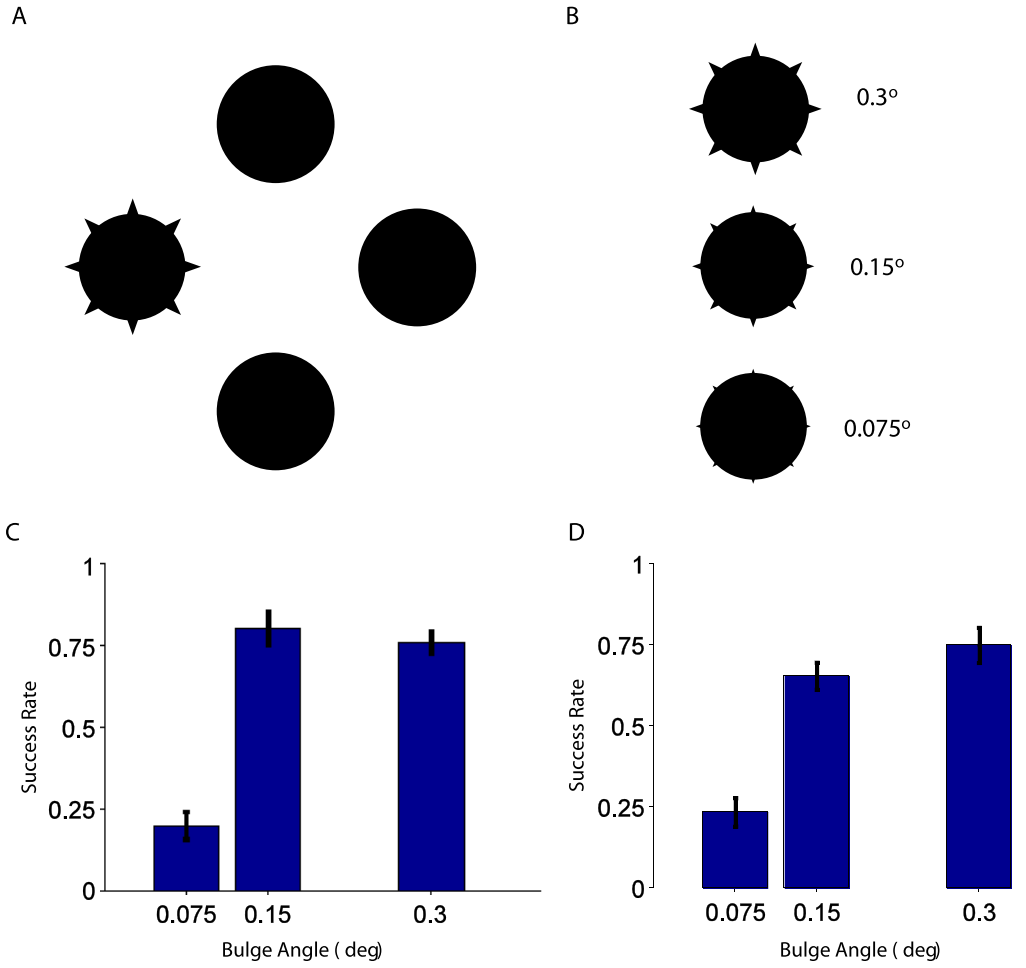

Figure 1. Behavioral exploration of visual acuity in archerfish. All targets were circular, except one that also contained small bulges at its circumference. A. To measure visual acuity we examined the ability of the fish to identify details in a target. This panel shows one example of target configuration that was presented in the experiment. The fish had to detect the target with bulges and to shoot at it. B. The relative sizes of the bulges under the different conditions. C and D. Shot success probability of the two fish. When the angle subtended by the bulges was 0.075°, both fish performed with a probability of success no better than chance; when the bulge subtended 0.15°, the probability of making a correct choice increased to ~0.75.

We measured this angle in two archerfish by a multiple choice experiment in which the fish were trained to identify a target with fine spatial details. Fish were presented with four targets on a computer monitor 57 cm above water level. All targets were disks, except one that also included small bulges along its perimeter (Figure 1A). Importantly, prior to the experiment the fish were trained to shoot at a *single* bulged target but to ignore purely circular ones, and after a week of training, they were tested with the multiple choice experiment. Each fish was tested with 60 such trials, and the three bulge sizes (see Figure 1B) were presented in these trials in equal probability and random order.

The success rates of the two fish at hitting the bulged target as a function of the angular size of the bulge are presented in Figure 1C and D. Based on these results and compared to the 0.25 chance level, it is possible to conclude that the detection threshold in archerfish or their minimum angle of resolution lies within the range of 0.075° and 0.15°. These values translate to a range from 6.5 to 13 μm on the fish retina for an eye with a 5 mm radius (measured by a caliper).

The effective radius of the archerfish area centralis devoted to encode spatial properties of a target

We explored, based on behavioral experiments, the effective radius of the archerfish area centralis. In these experiments we monitored eye movements while fish were tracking and shooting at a stationary-displaced target. We trained two archerfish to swim into a small region in the tank and to shoot at a black circular target presented on a computer monitor. The target

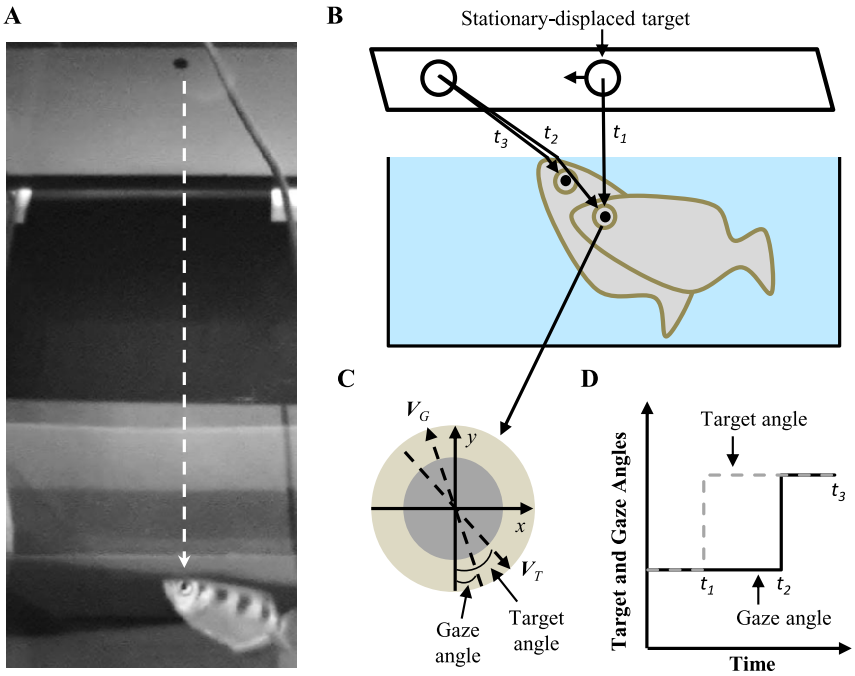

Figure 2. The experimental procedure to acquire the functional spatial angular width of the area centralis. A. An image of the fish and the target shortly before target motion onset. The target appeared 57 cm above the water level while the fish was swimming parallel and adjacent to the tank side that was facing the camera. Shortly after, the fish performed a saccade that shifted its gaze toward the target. Then the target was either displaced or moved forward, and on average, 0.7 s later the fish shot at it. In some of the trials the fish performed a second saccade before the shot. B. A diagram of the stationary-displaced target experiment. The times of target motion onset, saccade (if existed) onset, and the time of shot are indicated in the sketch as t_1–t_3, respectively. C. A diagram of the gaze and target angles on the fish eye. Both angles were measured on a plane (proximately parallel to the fish's sagittal plane) relative to the normal of the water surface. D. A diagram of the dynamics of the gaze and target angles during the experiments.

first appeared above the head of the fish (Figure 2A) and triggered the fish to perform a saccade that directed their gaze toward the target. Then, shortly after it first appeared, the target was displaced at various visual angles (Figure 2B). The fish then shot at the displaced target, sometimes with and sometimes without a second saccade.

Throughout all the experiments the fish swam freely while both their body position and the target position were recorded by a set of high-speed video cameras. These recordings were analyzed offline by custom written software (see Methods) to measure both the fish *gaze angle* (with 0.2° precision) and the *target angle* (with 0.1° precision) during the shooting process (Figure 2C). The first saccade after target onset reset both of these angles to zero. A schematic view of the angles' dynamics after target displacement (at time t_1) is depicted in Figure 2D.

Figure 3A presents the gaze angle of both fish as a function of target angle *at the time of the shot*. Trials having zero gaze angles (up to measurement error) exhibited no second saccade before the shot, and hence the maximum target angle that elicits no such second saccade was found to be 3° (depicted by the vertical dashed line). This behavior can also be seen by examining the saccade probability as a function of target angle (Figure 3B). For small target displacement this probability is low, and for high ones it is one. We chose a target angle threshold of ~3°, since for this angle the saccade probability is chance level. To summarize, whenever the target angle was larger than this threshold, a saccade was executed, suggesting that the quality of visual information significantly decreases above this eccentricity.

We can also examine these results from the fish perspective by introducing the *gaze-lag*—the angular difference between the target and gaze angles. This variable represents the angular distance between the image of the target on the retina and the region on the fish retina devoted to monitor a target before shooting at it, in analogy to retinal eccentricity. Gaze-lag measurements as a function of target angle at the time of shot are presented in Figure 3C. The horizontal dashed line represents the saccadic threshold of the gaze-lag borrowed from Figure 3A. It is evident that in the vast majority of trials, the fish tolerates gaze-lag values no larger than this value. This also becomes clear from the distribution of gaze-lag (at shot time) across trials (see Figure 3D, inset), which shows that the same threshold captures more than 93% of the

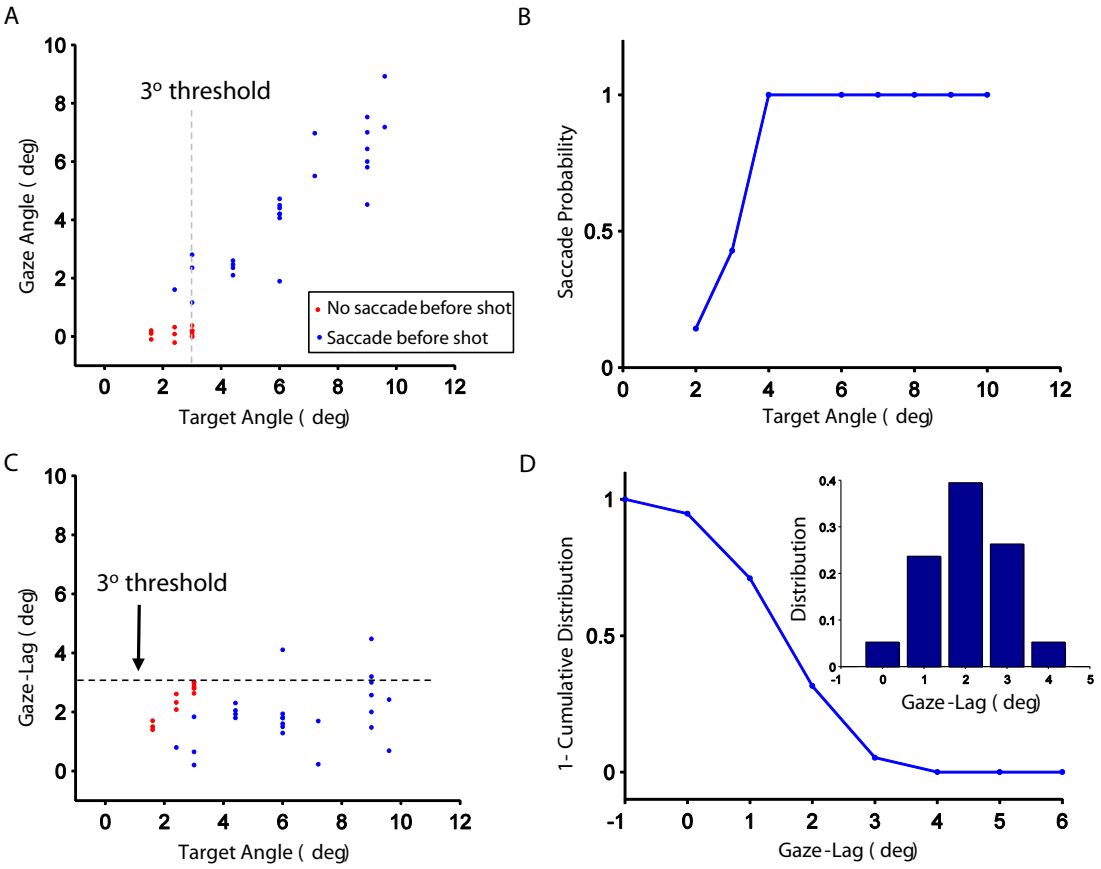

Figure 3. Measuring the functional angular width of the ventro-temporal area centralis. Gaze angle measurements as a function of target angle at the time of the shot in the stationary-displaced target experiment. Note the vertical dashed line at a target angle of 3° that represents a threshold of the target angle for saccade execution. B. Saccade probability as a function of target angle. At a target angle of ~3° this probability is at chance level, which suggests that for larger target angles, the fish visual acuity is reduced. C. Gaze-lag measurements as a function of target angle at the time of the shot. D. The complementary cumulative distribution of the gaze-lag and in the inset—the gaze-lag distribution. The complementary cumulative distribution represents the probability of the gaze-lag to be above a certain value. As can be seen in the figure, for gaze-lag above 3°, this probability is low, and for lower gaze-lag values, it sharply increases. This suggests, again, that visual acuity is severely decreased for gaze-lags above 3°.

cumulative distribution. An illustrative way to substantiate this threshold is by examining the complementary of the cumulative distribution (Figure 3D). This function represents the probability of a gaze-lag to be above a certain angle at the time of shot. As can be seen in the figure, for a small gaze-lag this probability is one, and as the gaze-lag increases, it sharply decreases to effectively vanish for a gaze-lag of >3°.

In summary, we found that for the purpose of target interception, the fish can tolerate angular displacement of up to ~3° from the initial location of the image of a target on the retina. Thus we suggest that this width represents an effective radius of the area centralis that is employed for monitoring stationary targets in high visual acuity. In the case of moving targets, this threshold is doubled and reaches the full radius of the area centralis (Ben-Simon, Ben-Shahar, Vasserman, & Segev, in press).

Accommodation in the archerfish

As suggested by Temple et al. (2010), to gain high visual acuity on targets, the archerfish employ an area centralis on the ventro-temporal retina. In addition the fish can accurately shoot at targets as small as few a millimeters from a distance that ranges from few centimeters above the water (at smaller distances, below their standard length, they can catch prey with their mouth by jumping out of water) up to a distance of ~1.5 m (Timmermans, 2001). These findings suggest a mechanism of accommodation in the fish eye that supports this type of behavior, probably through a process of contraction and relaxation of muscles that are connected to the lens. Such a process may enable them to focus an image of proximal and distant targets on the ventro-temporal retina. To examine this mechanism we performed magnetic resonance imaging

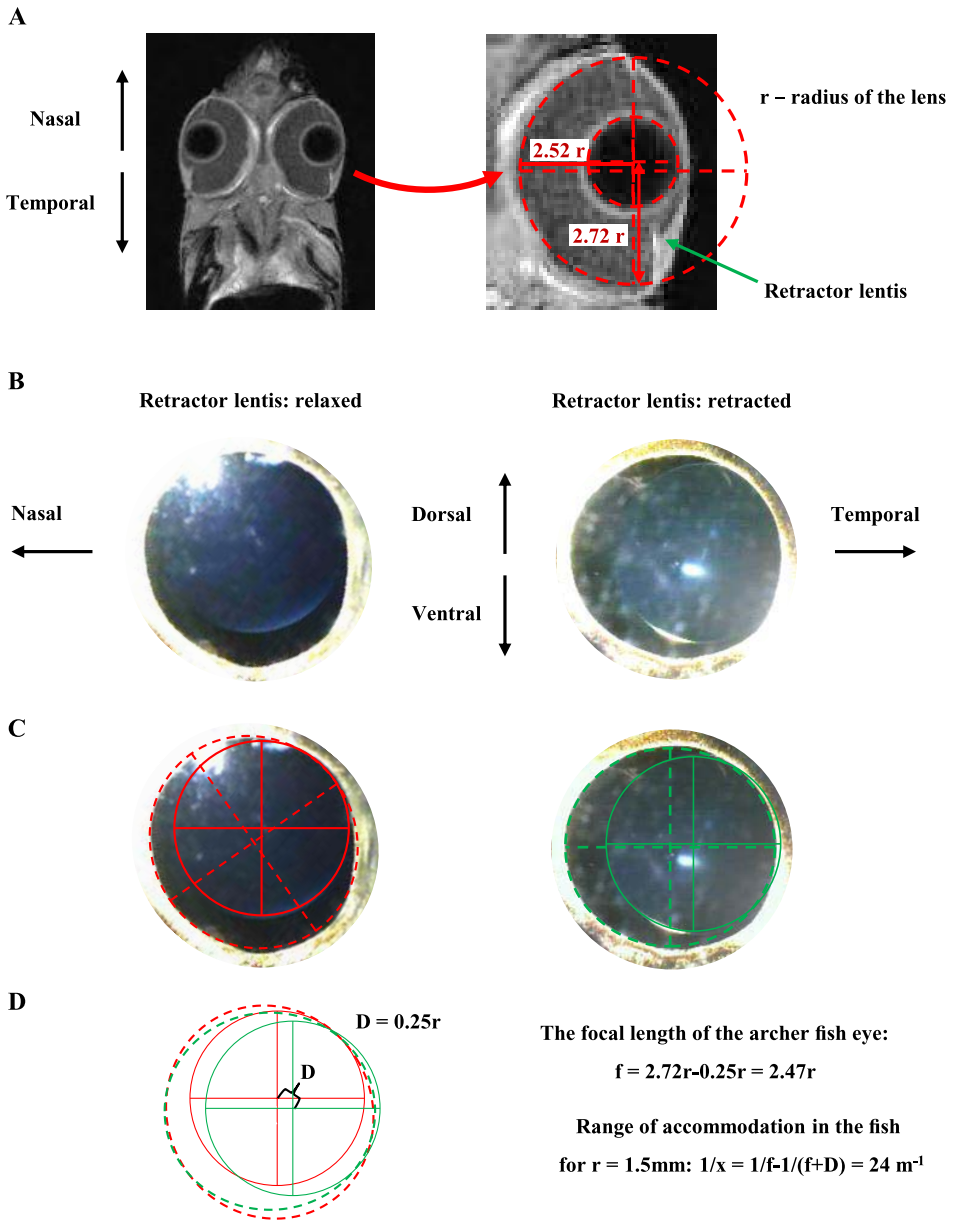

Figure 4. Accommodation in the archerfish. A. Left, horizontal cross-section MRI scans of the archerfish head and on the right, a magnification of the right eye. During a shooting sequence, the fish binocularly fixates on targets at various distances through contraction or relaxation of its retractor lentis (indicated). The two red straight lines sketched on the right image denote the distances from the lens center to the central and temporal retina. These distances were derived based on two circular fits (indicated in dashed red lines) to the retina and lens. B. Segments from two front view images of the iris of the eye of a fish that show the fish pupil and lens under two conditions: when the retractor lentis is relaxed (left) and retracted (right). C. The same segments, with additions of a circle and an ellipse on top of each image, which were fitted with the lens and pupil, respectively. Also indicated are the two main axes of each one of these ellipses. D. A diagram of the circles and ellipses from C, after alignment, which illustrates the retraction length (indicated by *D*, see Methods). Also shown are derivations of the focal length of the lens and the value of the range of accommodation.

(MRI) scans of the fish to explore the fish eye anatomy and took images of the lens in the intact fish.

We studied the gross anatomy of the eyes of recently dead fish in search for a muscle that can support such a mechanism (Figure 4A). The ability to detect such a smooth muscle in the MRI was nicely demonstrated in studies of accommodation in the human eye (Demer, Kono, & Wright, 2003; Strenk et al., 1999). We found that in the archerfish, as in other teleosts (Somiya & Tamura, 1973; Tamura & Wisby, 1963), there is a retractor lentis, a smooth muscle that is connected to the lens. The contraction and relaxation of this muscle (green arrow in Figure 4A), together with eye movements, enable the fish to bring targets within their

anterior and/or dorsal fields of view into focus on their ventro-temporal retina. In addition, we found no muscle medial or lateral to the lens, which implies no accommodation in the lateral field of view.

Based on the MRI images in which the retractor lentis was relaxed when the animals were dead (Tamura & Wisby, 1963), we found that archerfish, like many of teleosts, are myopic in the anterior field of view and hyperopic in the lateral field of view (Figure 4A). To acquire these results we measured the distance from the lens center to the temporal and central retina, in units of the lens radius, and found them to be 2.72 and 2.52, respectively ($SD = \pm 0.05$, $n = 3$). Note that the distance between the lens center and the central retina is in close agreement with the average Matthiessen's ratio of $f/r = 2.55$ (Sadler, 1973) where f denotes the focal length of the lens and r denotes the lens radius.

To measure the range of accommodation in the archerfish, we captured images of the fish eyes when they were restrained and later dead (Somiya & Tamura, 1973; Tamura & Wisby, 1963). When the fish were dead, using a condition similar to that used during the MRI scans, their retractor lentis was relaxed. When the fish were restrained, their lens moved towards the temporal retina (with inclination towards the ventro-temporal retina) by $0.25r$ ($SD = \pm 0.05r$, $n = 3$, see Figure 4B through D).

Combining the MRI results with the results of the accommodation, we found that in the anterior field of view, the distance from the lens center to the temporal retina ranges from $2.72r$ when the muscle is relaxed, to $2.47r$ when it is retracted (Figure 4C, D). Thus, the maximum accommodative change in the temporal direction in which a retinal image can be focused is 24 diopters (Figure 4D). That means that the archerfish can accommodate from ~4 cm to infinity. Based on these results and on fish behavior, we suggest that, typically, before shooting at prey, an archerfish fixates binocularly on it (Dill, 1977; Luling 1963; Plotkin et al., 2008) by retracting or relaxing the retractor lentis in both of its eyes. At that point the image of the prey is sampled by the ventro-temporal part of the retina, or more specifically, by the area centralis. This latter claim is discussed next.

The relationship between the image of target on the retina and the anatomically reported area centralis

For the area centralis to support high acuity vision, its anatomical location on the retina, as reported by Temple et al. (2010), should coincide with the image of target on the retina. Note that here the term "gaze" refers to the binocular gaze at a target during a shooting sequence. Several steps were required to confirm this hypothesis. First, we traced light rays from displayed targets to a geometrical model of a semisphere that represents the fish eyecup (Charman & Tucker, 1973; Easter, Johns, & Baumann, 1977; Schimidt, Cicerone, & Easter, 1978). We then aligned the fish retina relative to this model based on retinal landmarks such as the optic nerve and embryonic fissure. Combining the two steps we hence obtained the location of the image of target on the retina, which was found to be close to its edge (see green circle in Figure 5 and Methods). Note that the radius of this circle represents a variability of 1° SD in the measurement. Finally, by aligning the cone photoreceptor topographic map from Temple et al. (2010) on Figure 5, we could mark the area centralis boundary on the retina image (yellow curve) and reveal that the image of target on the retina is located near its center (green circle). We conclude that from this perspective, the area centralis is likely to facilitate high acuity vision in the archerfish.

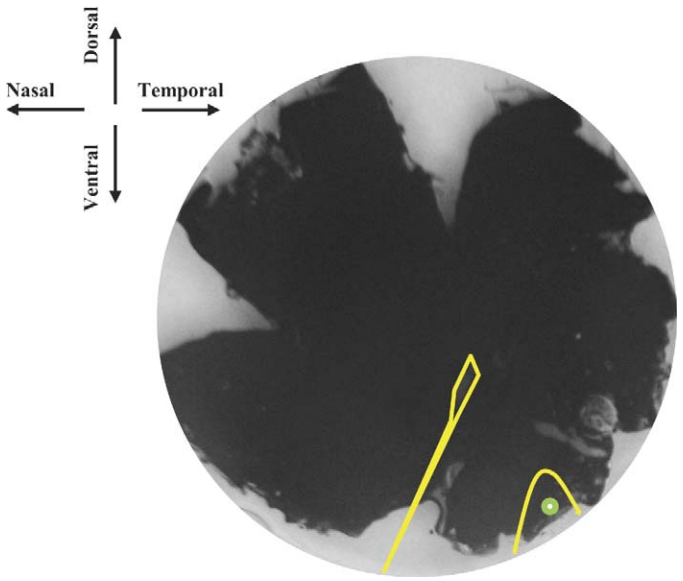

Figure 5. An image of the target on the retina is located at the center of the archerfish's anatomically reported ventro-temporal area centralis. A circular segment containing a front view image of the whole mounted retina of an archerfish. Overlaid in yellow are boundaries of the ventro-temporal area centralis (around the green dot) and outlines of the embryonic fissure. The green dot represents the measured location of the target image on the retina.

Anatomical factors determining archerfish visual acuity

The retina of the archerfish, similar to retinas of other vertebrates, is composed of five layers, as can be seen in the cross section in Figure 6A. As described before (Masland, 2001), two of these layers are critical

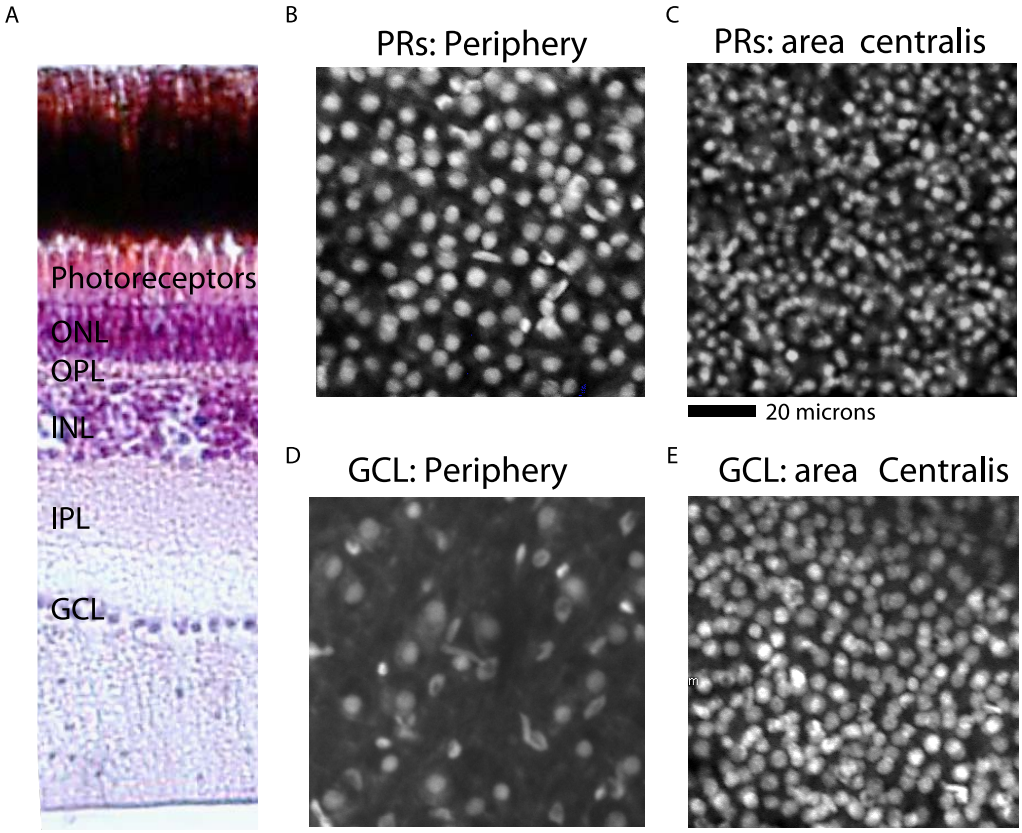

Figure 6. Photoreceptor and ganglion cell densities in the area centralis and peripheral retina. A. A cross section of the archerfish area centralis with indication of the photoreceptors and the five retinal layers: outer nuclear layer (ONL), outer plexiform layer (OPL), inner nuclear layer (INL), inner plexiform layer (IPL), and ganglion cell layer (GCL). B and C. Images of the nuclei of the photoreceptors in the periphery and in the area centralis, respectively. Density of photoreceptors was found to be as low as ~15,000 cells/mm^2 in the periphery and as high as ~30,000 cells/mm^2 in the area centralis. D and E. Images of the ganglion cells in the periphery and the area centralis, respectively. Density of these cells was found to be in the range of 5,000–15,000 cells/mm^2 in the periphery and ~30,000 cells/mm^2 in the area centralis.

for determining the threshold for the animal's visual acuity—the ganglion and the photoreceptors layers. Temple et al. (2010) measured the density of cell populations in these two layers in the retina of the archerfish and found a region with no rods but a high density of 50,000 cells/mm^2 for both cone and ganglion cells—presumably the area centralis. Assuming a mosaic organization of the cones, this density indicates an average spacing of 4.5 μm between cones in the area centralis, a measure that translates to a minimum angle of resolution of 0.057° for a fish with an eyeball radius of 4.5 mm. Here we attempted to independently reproduce these findings, in part to improve our ability to pinpoint the area centralis for the forthcoming electrophysiological measurements.

We measured the cellular density in the photoreceptor layer in various parts of the archerfish retina and found it to be ~30,000 cells/mm^2 in the area centralis and as low as ~15,000 cells/mm^2 in the peripheral retina (see Figure 6B, C). We note that these measurements do not distinguish rods from cones. However, assuming the area centralis contains no rods (Temple et al., 2010) while other regions contain them in high density, these results are consistent with Temple et al. (2010), at least qualitatively, with possible differences due to examination of other species of archerfish. Consequently, at the area centralis, this density translates to an average spacing between cones centers of 5.8 μm, with a minimum angle of resolution of ~0.073°.

One should keep in mind that after the image is sampled by the photoreceptors, it is resampled by the ganglion cells. Hence, next we measured ganglion cell densities in both the area centralis and peripheral retina (Figure 6D, E; see Methods). Ganglion cellular density in the peripheral retina was diverse: 5,000–15,000 cells/mm^2 (at other parts of the ventro-temporal retina), while in the area centralis it peaked at ~30,000 cells/mm^2. In other words, our measurements show that in the area centralis, the density of ganglion cells is the highest and similar to that of photoreceptors. This suggests that the area centralis, unlike other parts of the

fish retina, provides the highest visual acuity. In addition, in the area centralis there is no significant deterioration of the spatial resolution at the retinal output; however, this could also be the case in other retinal patches.

To summarize both behavioral and anatomical results, the minimum angle of resolution of 0.073° measured anatomically is comparable with the range of 0.075° to 0.15° we found behaviorally. An anatomical resolution that is smaller than the behaviorally measured one was also reported for human subjects (Rodieck, 1998), with behavioral performance being 1 min of arc while the anatomical one reported at approximately half this value (for an eye with a radius of 15 mm and cone center spacing of 2.3 μm in the fovea) (Rodieck, 1998).

The RF width in the area centralis can support high visual acuity vision

To conclude our study and complement the behavioral and anatomical findings with physiological evidence also, we measured the RF size of ganglion cells in both the area centralis and peripheral retina. Cell response (frequency of action potentials) was measured with an extracellular electrode while projecting to the photoreceptor layer a high contrast grating stimulus. The grating was composed of interleaved white and black bars that flipped at 1 Hz. Bar width (and correspondingly the spatial frequency of the pattern) was changed in 9 steps from 512 μm to 8 μm on the retina (Figure 7A; see Methods). Initially, when the bar is large, each cell is stimulated with a strong ON/OFF stimulus. As a result, cells respond with a high firing rate or with short spike latency (or both) after a grating flip. When the grating spacing is reduced and eventually becomes much smaller than the RF size, the cellular response is reduced down to spontaneous levels indicating that the cells are blind to such fine details. This reduced response was used to mark the size of the RF.

Rasters of representative cells from peripheral retina and the area centralis are shown in Figure 7B and C, respectively. The corresponding probability to generate at least one spike after a stimulus flip (all as a function of bar width) is shown in Figure 7D and E. The results indicate that the RF size of ganglion cells in the area centralis can be as small as 8–16 μm, which corresponds to —two to three photoreceptors in the retina and visual angular acuity of 0.1°–0.2°. This ratio is slightly higher than the corresponding ratio of 1:1, expected between ganglion and photoreceptor cells in the area centralis and may result from limitations in our measuring system (see Discussion). In the peripheral population the corresponding results indicate an RF size as large as ~350 μm that corresponds to 60 photoreceptors in the retina and a visual angular acuity of ~4°.

Finally, to further analyze the two populations of ganglion cells we examined the normalized spike probability by scaling the probabilities to measure a spike between zero and one and defining the RF size as 75% height of the normalized curve (Figure 8A, B). Examining the two populations, we found the RF size in the area centralis to be in the range of 8–50 μm and in the periphery in the range of 200–400 μm, which translates to angular widths of 0.1°–0.6° and 2°–4°, respectively (Figure 8C and D). The average width of each one of the two populations was 29 μm ($SD = 10$ μm) and 290 μm ($SD = 100$ μm) in the area centralis and the periphery, respectively (Figure 8E). In other words, this is yet another indication that ganglion cells in the area centralis can report to the brain on fine visual structures.

Discussion

We examined visual acuity in the archerfish through behavioral, anatomical, and electrophysiological measurements. Behaviorally, we showed that target detection is in the range from 0.075° to 0.15° with an average value of about 0.11°. This resolution was suggested to be set by a specialized region in the fish retina, the area centralis, devoted to encoding targets with high resolution. Anatomically, we measured cellular densities of both photoreceptor and ganglion cells in the area centralis and in the peripheral retina. For both cell types the density peaked at the area centralis to a value of ~30,000 cells/mm^2. This value can yield a minimum angle of resolution of 0.073° that is comparable with the one we found behaviorally. Indeed, these results are somewhat smaller than densities reported in an earlier study on other archerfish species (Temple et al., 2010). However, this could be expected from between-species differences, or slight differences in the preparation procedures that lead to shrinkage of the tissue.

To validate that the archerfish use their area centralis for the detection of the targets, we employed geometrical ray tracing from targets above water level to show that the image of target on the retina coincides with the area centralis. Moreover, we examined their accommodation mechanism (Figure 4). This mechanism is based on relaxation or retraction of their retractor lentis, the smooth muscle that is connected to the lens, that thus enables them to fixate on targets, near or far, respectively, in their anterior field of view.

In addition to behavior and anatomy, we also employed functional measurement of the RF size in the area centralis and peripheral retina and found them to be in the range of 0.1°–0.6° and 2°–4°, respectively.

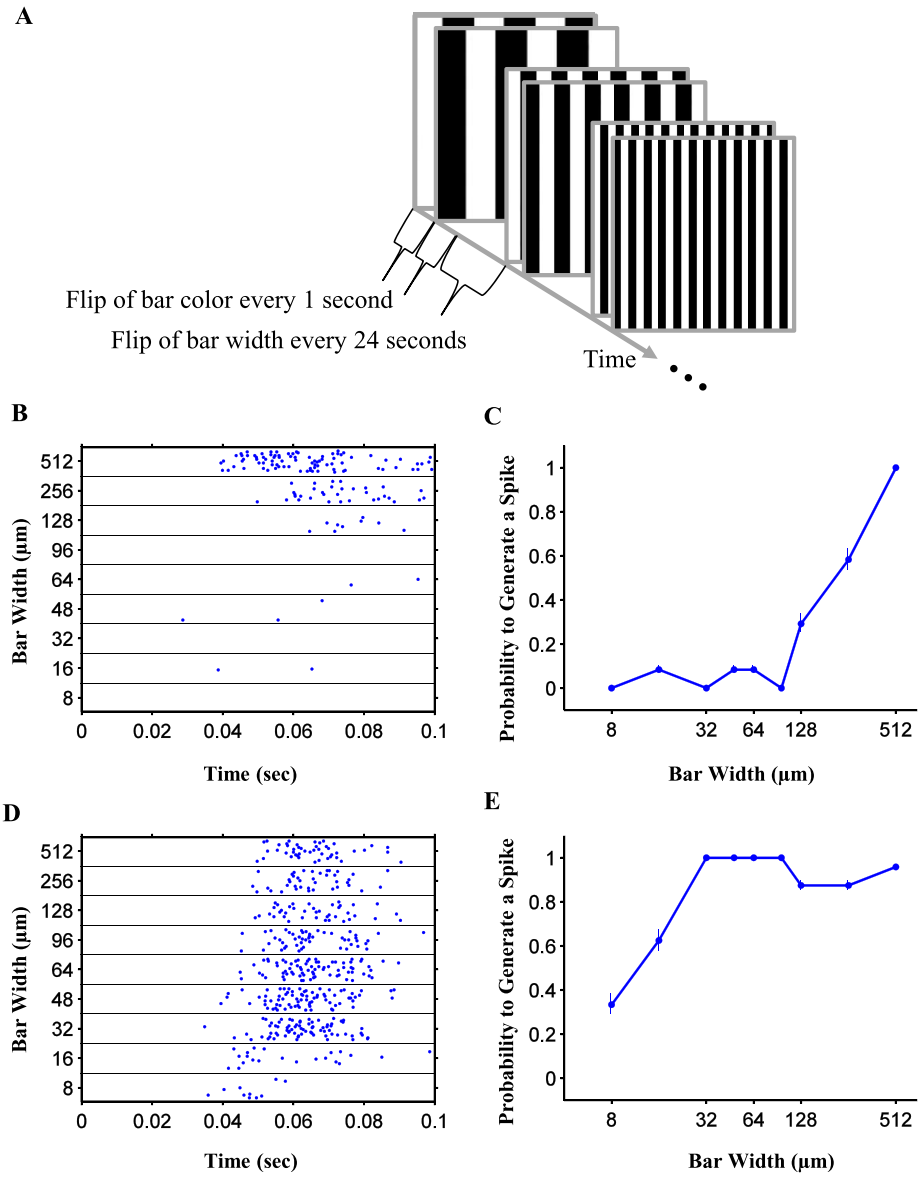

Figure 7. Electrophysiological measurements of ganglion cells responses to stimulus bar width in the area centralis and the periphery. A. The stimulus employed in the electrophysiological experiment. The stimulus was a grating composed of white and black bars that switched positions with each other each second. The grating spatial frequency was changed every 24 seconds with bar width on the retina of 512, 256, 128, 96, 64, 48, 32, 16, and 8 μm. B. Responses of ganglion cells to stimulus bar width as a function of time. These measurements were recorded from the peripheral retina. C. Probability to generate at least one spike as a function of bar width for the data presented in panel B. D. Responses of ganglion cells to stimulus bar width as a function of time. These measurements were recorded from the area centralis. E. Probability to generate at least one spike as a function of bar width for the data presented in panel D.

We found the width of the ganglion cell RF in the area centralis to be as small as two to three photoreceptors on the retinal plane. In this case we examined individual ganglion cell responses to the spatial properties of the stimulus that was changed on one axis while ignoring the case in which there are connections between the ganglion cell and photoreceptors on the vertical direction. Considering both cases implies that each such ganglion cell may collect information from about four to nine photoreceptors in the total area of the RF.

Although we did not find a 1:1 correspondence between the photoreceptors and ganglion cells, such a relation may indeed exist, but may not have been found due to technical limitations of our measuring system. For example, the side length of each pixel of the stimulus in our experimental system that is projected on the retina equals 8 μm, which may have bound the measurements of the RF width we could measure to a minimum of two photoreceptors. In addition, to stimulate a single photoreceptor, which is connected to a ganglion cell from which we record electric signals,

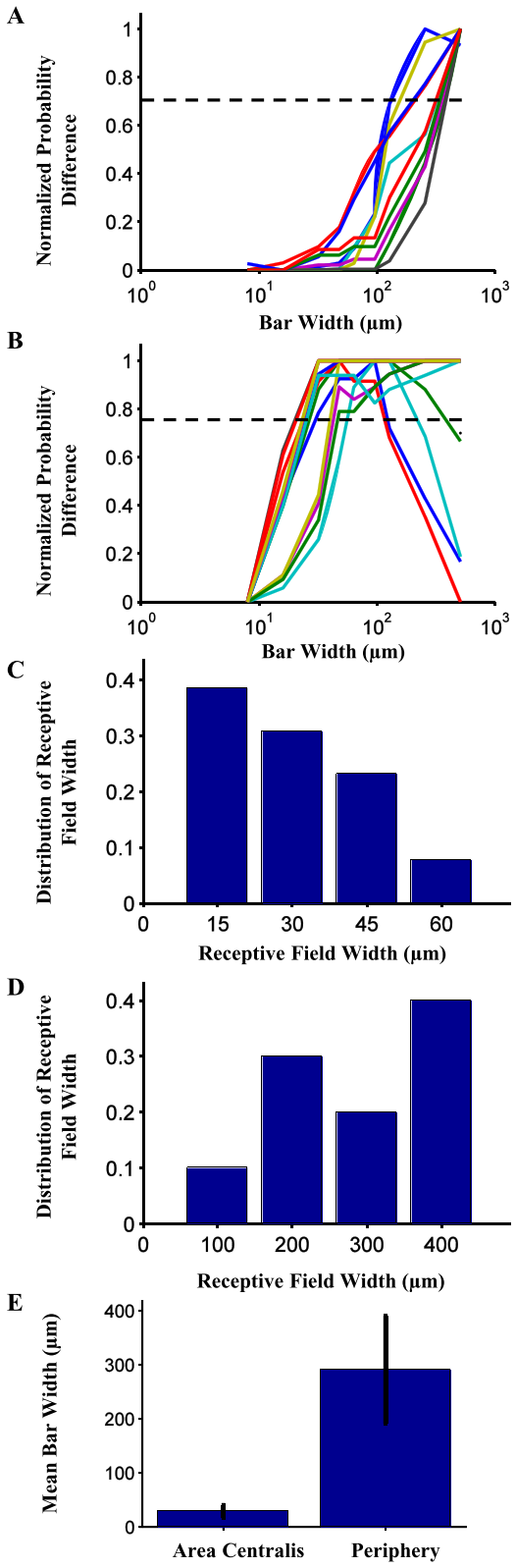

Figure 8. Electrophysiological measurements of the width of RFs of ganglion cells in the area centralis and the periphery. A. Normalized probability difference as a function of bar width in the area centralis (the various colors represent different cells). To derive this measurement we normalized the spike probability by setting its minimum to zero and its maximum to one (abscissa on the center of one of the bars in the grating stimulus with the 8 μm bar width should coincide with the center of this photoreceptor, a condition that may occur at a low probability. However, the smallest RF widths may be of two or more photoreceptors, which would then suggest an overlap in the RF of adjacent ganglion cells in the area centralis (see below).

Spatial resolution of the visual system can be limited by the optics of the eye due to diffraction, by photoreceptor spacing that limits the sampling frequency, and by the neural properties of retina or the brain (Neumeyer, 2003). In humans, the optical limit and photoreceptor spacing are within nice agreement of 1 min of arc. However, in fish, the optical diffraction is usually not a limiting factor for acuity (Land & Nilsson, 2012). In particular, the diffraction limit for green light in the archerfish eye (assuming 2.5 mm pupil radius) is ~0.46 min of arc or ~0.7 μm on the retina. This is clearly far better than the sampling limit set by the photoreceptors. Thus, visual acuity in the archerfish is governed by the photoreceptors or other properties of its visual system.

Another limiting factor of visual acuity is the resolution with which information streams to the brain via the retinal ganglion cells. A smaller RF may transfer more accurate information. However, one should keep in mind that there is no direct connection between ganglion cell RF sizes and visual acuity. In principle and in practice, RFs can overlap (Segev, Puchalla, & Berry, 2006). Thus by comparing the relative spiking of two or more cells with overlapping RFs, the brain can infer the fine details of an image feature that are smaller than the RF size of ganglion cells. Thus there is a complicated relationship between RF sizes, the extent of overlap between RFs, and noise.

Methods

Measuring eye movements in the stationary-displaced target experiment

Behavioral setup

All experiments were conducted in accordance with Ben-Gurion University of the Negev regulations and State of Israel laws on animal care and experimenta-

← logarithmic scale). B. Normalized probability difference as a function of bar width in the periphery. C. Distribution of the RF widths in the area centralis. To derive these widths we interpolated the bar width at 75% of the scaled probability difference. D. Distribution of the RF widths in the periphery. E. Mean values of the RF widths in the area centralis and the periphery.

tion. We trained two archerfish (*Toxotes jaculatrix*) to swim into a small confined region in the tank, while their bodies' sagittal plane was parallel to one of the tank sides (Figure 2A). When the fish were at that position, a black circular target with a diameter of 1.2 cm on a white background appeared above the their heads through a computer monitor (BX2235, 22″ LED backlit monitor, Samsung, Seoul, South Korea), positioned 57 cm above water level. After target appearance, the fish performed a saccade, and shortly after, but before the fish attempted to shoot at it, the target was displaced forward at various visual angles in the fish's sagittal plane, where it remained until the fish shot at it, with or without a preceding second saccade (Figure 2B). (Stimuli were created using the Psychophysics toolbox in Matlab; Brainard, 1997). In this manner when the fish made the second saccade, their eyes, which are located on the sides of their head, rotated primarily in a plane that was approximately parallel to the fish's sagittal plane. Such eye rotations around an axis perpendicular to the center of the pupil were used to obtain gaze angle. We referred to this rotation of the eye as *roll*, after one of the three angles that are commonly used to describe rotations (i.e., roll, pitch, and yaw; see Landau & Lifshitz, 1982).

Three high-resolution, high-speed video cameras (SI-1920HD, 120 fps, 1500 × 800 pixels/frame, Silicone Imaging, East Arques Avenue Sunnyvale, CA) were used to record behavior. The cameras were positioned facing one side of the tank, approximately 80 cm from the glass and 2 cm below water level. The cameras were assigned two functional modes. One camera monitored the entire scene, i.e., both the fish and the computer monitor. The second and third cameras, which were used for eye movement measurements, were both facing the front side of the tank to minimize image distortion due to air-glass-water refraction. In this manner the image plane of these cameras (i.e., their charge-coupled device [CCD] sensor) was approximately parallel to both the side of the tank and the fish's sagittal plane. To image the fish eye at maximal resolution, the field of view of these cameras (i.e., zoom level) was set close to the diameter of the eye.

To extract the gaze (or roll) angle from the video recordings, we developed a Matlab program that automatically analyzed each frame from each trial. First the program segmented the fish eye in each frame. Then the pupil was detected (by searching in the frame for the best fit with an ellipse pattern that represents the fish eye) and fitted with an ellipse in order to localize its center. The maximal circular patch centered around this point and fully contained in the eye segment was then extracted for further processing. We aligned all these circular patches from all frames according to their pupil center and took advantage of the presence of pigmented patterns on the fish iris in order to detect saccadic rotations. For each segmented frame, E_i, we calculated its edge map. Then, we searched for the rotation angle, θ, that would yield the best match to the edge map of the first frame, E_1. Specifically, if $R(\theta)$ denoted the rotation matrix for a rotation of the edge map around its center by an angle of θ, we defined the rotation of the eye at frame i as the value $\theta(i)$ that minimizes the measure $D(\theta) = \sum_{(x,y)\in 0}^{n} | R(\theta)\ E_i - E_1 |$, namely, the rotation that would best match the edge maps of the first and i^{th} frame via the L_1 norm. We applied this procedure for both cameras, and the final eye rotation at each frame was determined by averaging the results from both. We determined the accuracy of these measurements based on the distance of corresponding pixel points on the edge maps of E_1 and E_i, which were located at an average distance of 80 pixels from the pupil center. Note that these points represent the contour of the stripe that is located between the pupil circumference (with a radius of ~60 pixels) and the eye circumference (with a radius of ~100 pixels). For a single corresponding point we would have obtained a standard deviation of 1/80 rad or ~0.71°. However, we derived the rotation $\theta(i)$ based on at least 10 corresponding pixel points, thus improving the accuracy to ~0.22° by introducing a standard error estimation, which was done by multiplying the standard deviation by $1/\sqrt{n}$, where n denotes the number of the pixel points chosen.

The fish eye rotations are composed of a combination of roll and nonroll (i.e., pitch and yaw) rotations. When we measured the fish eye movements, we considered only the roll component of the eye rotation. In order to verify that the roll component captures most of the eye rotation, we also measured the nonroll component of the eye movements. These measurements were based on measuring the displacement in the center of the pupil that was induced by the second saccade. If this eye rotation is composed only from roll eye rotation, then the location of the pupil center would not change due to the saccade. However, a nonroll eye movement would induce a displacement of the pupil center. We measured this displacement based on frames that were captured before and after the second saccade and denoted it by l. To measure the magnitude of the eye rotation that was induced by the pupil displacement, we translated l into a metric unit (1 pixel = 0.05 mm) and divided it by the eye radius (5 mm). The arc tangent of this ratio represents the nonroll rotation of the eye. Based on the width of a single pixel (0.05 mm) and the eye radius (5 mm), we obtained a resolution of 0.57°. Doing so, we calculated the contribution of the nonroll component to the total eye rotation in all trials where the fish performed the second saccade, and throughout the data analysis we considered only those trials in which the contribution of the roll rotation was

>90% of the total eye rotation. Overall, this was the case in 90% of all trials.

Aligning the image of target on the retina with the anatomically reported area centralis

Two steps were used to obtain this result. First we identified the part of the archerfish retina on which targets above water level are projected during preying behavior. To this end we employed part of the video recordings from the stationary-displaced target experiment, which contained frames captured shortly after the first saccade. Recall that the first saccade was triggered by target appearance, thus we assumed (and verified, as presented below) that at that time, the fish directs its gaze toward the target. Based on images from these recordings and employing ray tracing from the target to a geometrical model of the fish eye, we found the projection of the target on the eye model. Then, to find where this projection falls on the retina, we aligned and mapped an image of the latter, including its area centralis, onto the eye model. All these steps are described next in details.

In our analysis, we assumed for simplicity that the fish eye is well approximated as a semisphere around a 3D coordinate frame (Charman & Tucker, 1973; Easter et al., 1977; Schimidt et al., 1978). The origin of the frame, denoted as eye frame, was set to coincide with the center of the lens at the center of the semisphere. The x-y plane was set parallel to the base of the semisphere with the y-axis set parallel to the pigmented stripe that traverses the iris. A diagram of the x-y plane of the eye frame superimposed on a front view of the iris of the fish eye (taken parallel to the iris plane of a constrained fish) is presented in Figure 9A (left panel). Note that in order to define the orientation of the y-axis relative to the stripe we employed an edge map of the image in Figure 9A, left panel, which contained the stripe. Then we searched for a straight line that passes through the pupil center and divided the stripe into two parts with the highest mirror symmetry (via the L_2 norm, i.e., the least squares method). To determine the direction of the y-axis relative to the anatomical axes of the eye we measured the direction of the y-axis of anesthetized fish and found it to be approximately parallel to the dorsal axis, which makes the x-axis parallel to the temporal axis. The z-axis was set to be perpendicular to the x-y plane and therefore to pass through the center of the pupil/lens and perpendicular to the base plane of the semisphere.

To measure the target projection on the eye model, we also needed to define a coordinate system common to both the target and eye model, denoted as a global frame. The origin of this system was set at the center of the lens, its y-axis set normal to the water surface and towards the target, and its z-axis set normal to the face of the tank in the direction of the camera. Hence, by construction, the x-y plane of this coordinate system was parallel to the CCD sensor. A diagram of the axes of the global frame, the fish, and the experimental setup is presented in Figure 9A (right panel). Having this modeling infrastructure, we measured the postsaccadic orientation of the eye frame relative to the global frame. For this purpose, we defined a reference orientation in which the eye frame is aligned with the axes of the global frame. Then we extracted the angles that were required to rotate the eye frame from the reference orientation to the postsaccadic one. A drawing of the eye model in both orientations (i.e., the reference and the postsaccadic) is presented in Figure 9B. Notice that the eye frame rotations around the x-, y-, and z-axes of the global frame correspond to the pitch, yaw, and roll, respectively.

We measured the pitch, yaw, and roll angles of the eye frame based on the front view image segment (Figure 9C, upper panel) and the postsaccadic segment (Figure 9C, lower panel). To measure the roll angle, we first identified the contour of the stripe on the iris in both segments. Then we rotated the contour of the front view segment around the z-axis of the global frame to match it with the postsaccadic one, and the angle we extracted for this rotation was the roll angle (Figure 9C).

To measure the pitch and yaw angles, we first rotated the front view segment around the z-axis of the global frame (by the roll angle we described above). Then we matched the pupil contour in both the front view segment and the postsaccadic one with two ellipses, aligned these ellipses around their centers, and measured the pitch and yaw rotations that are required to match the ellipses (Figure 9D).

The average values of the pitch, yaw, and roll angles were $-8.6°$, $5.8°$, and $36.2°$, respectively, and their standard deviations were $<1°$ (Figure 9E). The convergence of these measurements to a small region in the pitch, yaw, and roll space indicates that in all trials, the fish employs a small and singular region on its retina to monitor the targets after the saccade.

Ray tracing of the target projection on the retina after the saccade

To derive the location of the image of the target on the eye model, we examined the relation between a ray from the target and the eye frame in its postsaccadic orientation. For this purpose, we followed the translation of the target projection on the eye model from the reference orientation to the postsaccadic one due to the pitch, yaw, and roll rotations. At the reference orientation a ray from the target was in the direction of the y-axis of both the eye frame and the global frame (see Figure 9A, right panel); thus the target projection

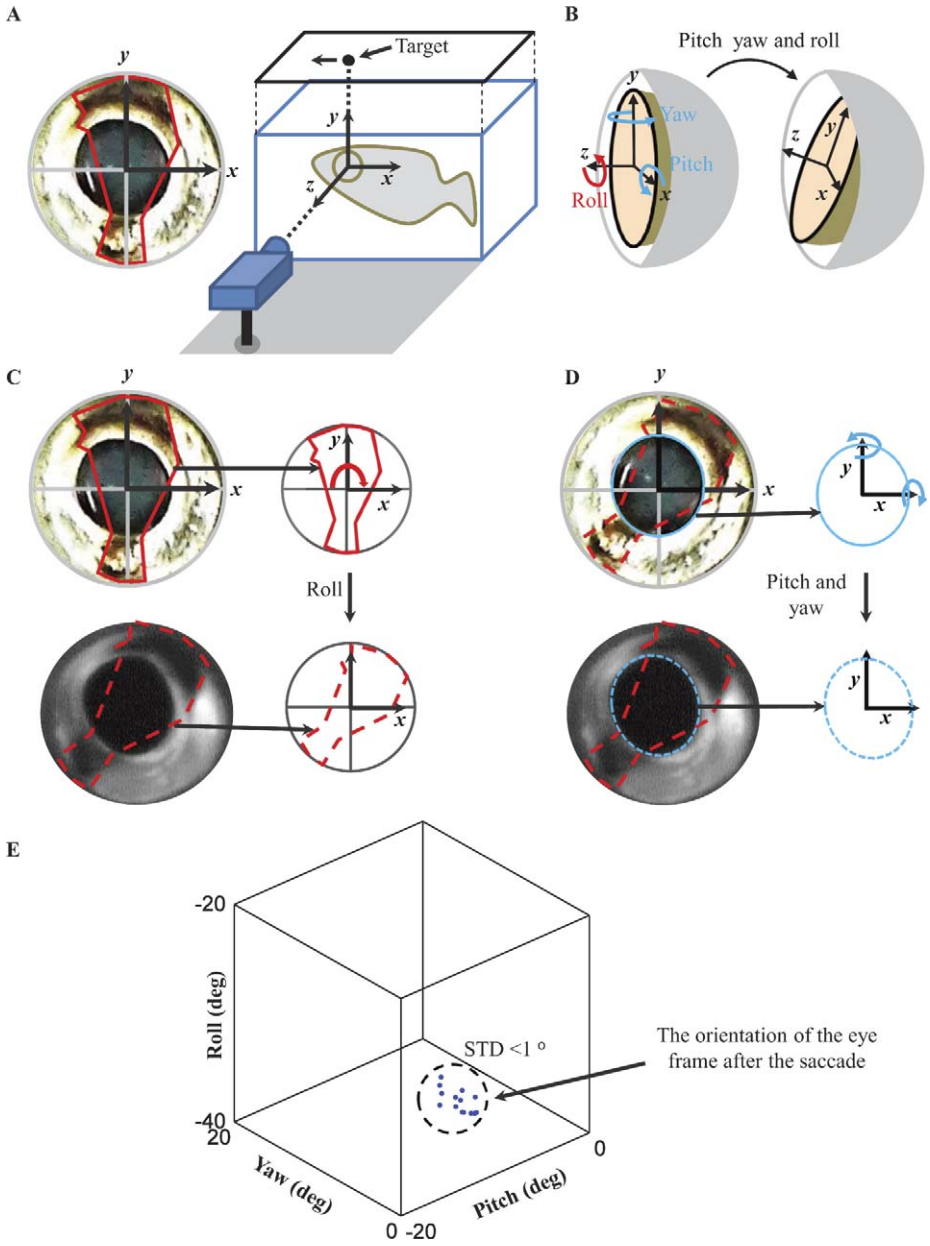

Figure 9. The fish monitors a target above water level using a small area on its retina. A. Left panel, drawing of *x*- and *y*-axes of the frame of the eye model on a segment containing a front view image of the iris of the fish eye (taken parallel to the iris plane). Right panel, diagram of the axes of the eye coordinate system, the fish, and the experimental set-up. To extract the fish eye orientation after it shifted its gaze toward the target, we employed a model of the eye that consisted of a frame with three perpendicular axes surrounded by a sphere. We measured the rotation of the frame from a reference orientation, in which it is aligned with the coordinate system to its postsaccadic orientation. B. A diagram of the frame in the reference orientation and the postsaccadic one. Here we refer to the rotations of the reference frame around the *x*-, *y*-, and *z*-axes as pitch, yaw, and roll, respectively. C. Upper and lower left panels: two segments containing images of the eye in the reference orientation and in the postsaccadic one, respectively. Upper and lower right panels: the contour of the stripe on the iris in the two segments relative to the *x*-*y* plane of the coordinate system. To measure the roll angle of the frame we rotated the contour of the segment of the front view image around the *z*-axis of the coordinate system to match it with the one of the postsaccadic segment, and the angle we extracted for this rotation is the roll angle. D. Upper and lower left panels: the two segments and on top, sketches of ellipses that were fitted to the contour of the images of the pupils in the segments. The front view image segment was rotated around the *z*-axis according to the roll angle. Upper and lower right panels: the two ellipses from the two segments relative to the *x*-*y* plane of the coordinate system. To measure the pitch and yaw, we rotated the ellipse of the front view segment around the *x*- and *y*-axes of the coordinate system to match it with the postsaccadic one. The rotation angles that we extracted for this match are the pitch and yaw. E. The mean values of the pitch, yaw, and roll of the frame in its post saccadic orientation were −8.6°, 5.8°, and 36.2°, respectively, and their standard deviations were <1°. The convergence of these measurements to a small region in the pitch, yaw, and roll space indicates that in all trials the fish employs a small and singular region on its retina to monitor the targets after the saccade.

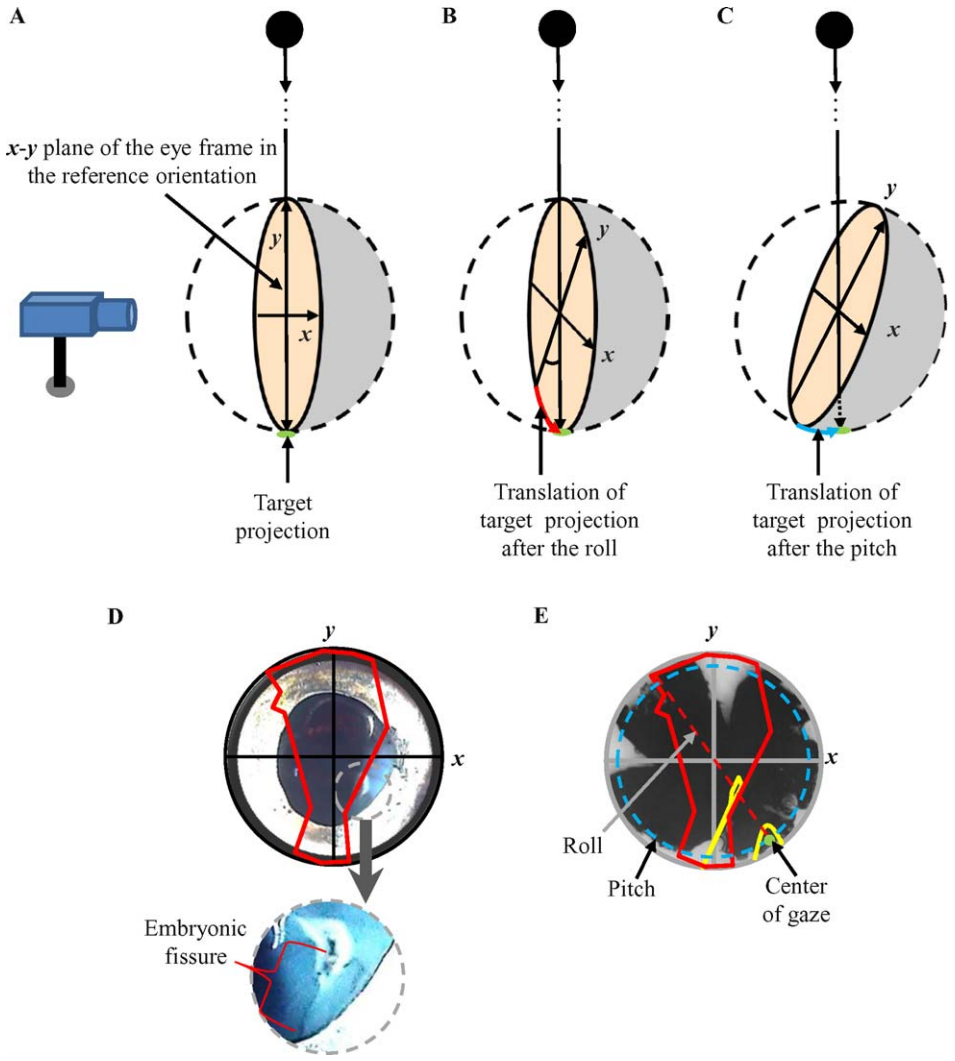

Figure 10. The archerfish image of target on the retina coincides with its anatomically reported ventro-temporal area centralis. A. A diagram of the camera and the eye model in the reference orientation as well as the target projection on the eye model (green ellipse). B. A diagram of the eye model after the roll of the frame. Notice the translation of the target projection on the sphere surface (red arrow). C. A diagram of the eye model after the pitch of the frame. Notice the translation of the target projection on the surface of the sphere (blue arrow). Based on these two rotations we found the position of the target projection on the eye model in the reference orientation. D. Upper panel, a segment containing a front view image of the iris of the fish eye. From the eye, the cornea, lens, and vitreous humor were dissected free to enable a clear view of the embryonic fissure. On top are drawings of the *x*- and *y*-axes of the coordinate system and of the contour of the stripe on the iris. We aligned the segment relative to the *x*-*y* plane by matching the contour of the stripe in the segment with that of the eye in the reference orientation (Figure 9A, left panel). Lower panel, zoom on the segment of the embryonic fissure. E. A segment containing a front view image of a flat-mount retina. On top are sketches of the contour of the stripe on the eye (in the reference orientation) and of the embryonic fissure (in yellow), as well as the *x*-*y* plane of the coordinate system. The segment of the flat-mount retina was rotated around the *z*-axis to set its embryonic fissure in the same orientation as the one in panel D. A red dashed line, which is rotated by 36.2° around the *z*-axis, represents the direction of the target relative to the *y*-axis due to the roll. A dashed light blue circle represents eccentricity from the center of the retina of 81.4° due to the pitch rotation.We denote the target translation due to the pitch by eccentricity since the flat-mount retinal segment represents the retina in the *x*-*y* plane and the translation was along the *y*-*z* plane of the retina. The point of intersection between the red line and the blue circle (indicated by a green circle) represents the position of the image of target on the retina. The yellow curve that confines this circle represents the boundary of the area centralis of the fish eye. This boundary was extracted based on cone density map of the archerfish retina (see Methods).

fell on the "south pole" of the eye frame (Figure 10A). The roll rotation rotated the eye frame by −36.2°, which corresponds to the angle between the *y*-axis of the eye frame (in the global orientation) and the direction of the target projection, in the *x*-*y* plane (Figure 10B). This rotation translated the target projection from the "south pole" of the eye frame, on the sphere surface of the eye model, along the *x*-*y* plane, at 36.2° of arc distance (see Figure 10B, red arrow). The pitch rotation rotated the eye frame by −8.6°, which resulted in a second translation of the target projection, on the sphere surface, along the *y*-*z* plane of the global frame, at 8.6° of arc distance (see Figure 10C, blue arrow). Note that the target projection after this rotation was at an eccentricity of 81.4° from the point of intersection between the eye frame negative *z*-axis and the sphere. The yaw rotation rotated the eye frame by 5.8°; however, this rotation is small relative to the other two (of ~0.2 mm of arc distance), and for simplicity we neglect it.

To find the orientation of the retina relative to the eye frame, we first dissected free an isolated eye of an archerfish and removed from it the cornea, lens, and vitreous humor. This procedure enabled a clear view of the embryonic fissure of the retina. Next, we captured a front view image of this isolated eye and extracted from it a circular segment containing only the eye. Then, we rotated this segment around the pupil center to match the stripe on the iris there with that of the front view segment of the eye (Figure 10D). Following this we dissected a retina free to prepare a flat-mount retina, captured a front view image of it, and extracted from the image a circular segment containing only the flat-mount retina. Finally, we aligned the segment of the flat-mount retina relative to the eye frame (see Figure 10E). This was done based on the orientation of the embryonic fissure relative to the eye frame in Figure 10D.

To identify the image of target on the retina, we incorporated to Figure 10E the position of the target projection relative to the eye frame. Notice in the diagram of the dashed red line that is rotated around the *z*-axis at 36.2° relative to the *y*-axis of the frame. This line represents the direction of the target projection after the saccade relative to the frame as a result of the roll. Another diagram given is of a dashed blue circle that denotes an eccentricity of 81.4°. This circle represents the direction of the target projection after the saccade relative to the eye frame as a result of the pitch. The intersection of the red and blue lines (indicated by a green circle in Figure 10E) represents the location of the image of the target on the retina. Finally, we matched the image of the retina with the archerfish cone photoreceptor topographic map to explore whether the image of the target on the retina coincides with the anatomically reported area centralis of the archerfish and found that the two regions indeed coincide (Figure 10E).

Retinal cross section preparation

Isolated retinal tissue was fixed in 4% paraformaldehyde overnight and dehydrated gradually through a series of increasing alcohol concentrations. Tissue was cleared and embedded in Paraplast (Kendall, Mansfield, MA) according to conventional procedures (Ventura et al., 2009). Sections of 7 μm were cut onto silane-coated slides (Menzel-Gläser, Braunschweig, Germany). Prior to the histological procedures, the slides were deparaffinized in xylene and rehydrated gradually through a series of decreasing alcohol concentrations. Later slides were stained with hematoxylin and eosin using standard staining protocol (http://www.ihcworld.com/_protocols/special_stains/h&e_ellis.htm).

Whole retina preparation

The isolated retina was transferred to 4% paraformaldehyde in phosphate-buffered saline (PBS) for 20 min. The tissue was then incubated in 4% paraformaldehyde containing 0.1% Triton X-100 in PBS for an additional 20 min, washed three times in 0.1% Triton X-100 in PBS, and then stained with 5 mg/μl Hoechst (Sigma, Cat #861405) overnight at 4°C and afterwards washed three times in 0.1% Triton X-100 in PBS and then placed on a slide and mounted in Citifluor glycerol (Ted Pella, Redding, CA). A coverslip was placed, and the preparation was sealed with nail polish. Confocal images were taken on an Olympus FV1000 laser-scanning confocal microscope (Olympus, Tokyo, Japan).

Electrophysiology of retinal ganglion cells

Archerfish retinas were isolated from the eye in the dark after a period of 1 h of light adaptation. Each retina was peeled from the sclera together with the pigment epithelium and placed in a petri dish with a glass bottom, with the ganglion cell layer facing down. Retinas were superfused with oxygenated (97% O2 and 3% CO2) Ringer's medium (120 mMNaCl, 2.5 mMKCl, 1 mM $MgCl_2$, 0.7 mM $CaCl_2$, and 3 mM $NaHCO_3$) at room temperature (Segev et al., 2007). A sharp electrode (~1 MΩ impedance, Alpha-Omega cat # 366-060620-11) was lowered onto the retina from above by means of a standard mechanical manipulator. Extracellular signal was amplified and digitized at 15 kSamples/s and stored for off-line analysis. Spike sorting was done by extracting from each potential waveform amplitude and width, followed by manual clustering using an in-house written Matlab program.

Data from seven retinas taken from six different animals are presented (total number of cells used 23).

Stimulus

The stimulus for in vitro retinal preparation was presented on an LCD monitor (2233RZ, 120 Hz, Samsung). The stimulus was an ON/OFF grating with changing bar width (512, 256, 128, 64, 48, 32, 16, and 8 μm) on the retina.

Accommodation in the archerfish

MRI measurements of three archerfish were acquired at 1T by means of an Aspect M2 high performance MRI system (Aspect Imaging Technologies Ltd., Shoam, Israel). The system is equipped with a 35 mm solenoid Tx/Tr coil (inner diameter 35 mm) and fast gradient coils (gradient strength, 450 mT/m at 60 A; ramp time, 250 μs at 160 V). Anatomical MR images were acquired using a standard T2-weighted fast spin echo sequence, with TR/TE/NEX = 2000/74/4. Multislice axial scans were collected with a 5 cm field-of-view (FOV) and data matrix of 256 × 256, resulting in a 0.195 mm in-plane resolution, slice thickness of 1 mm. To measure the distances from the lens center to the central and temporal retina and to measure the lens radius, we fitted both the lens and the retina in the images with circles (Figure 4A).

To measure the length of the retractor lentis retraction, we captured front view images of the iris of the eyes of three fish once when they were restrained and their retractor lentis was contracted and later when they were dead and the muscle was relaxed. To measure the length of retraction between the two conditions, for each fish we fitted the segment of the pupil and lens from its images, taken when it was alive and dead, with ellipses and circles, respectively (Figure 4B, C). Then we matched the two ellipses by aligning their centers (Figure 4D). To measure the distance from the centers of the two lenses, which represents the retraction length, we subtracted the distance between the centers of the ellipse and its corresponding circle in the two cases. The absolute value of this difference represents the length of the retraction of the retractor lentis. To validate that, our approach of measuring the retraction length based on the matching of the two ellipses is correct, we also matched between segments of the circumference of the iris under the two conditions and found the retraction lengths to be about the same.

In our ray tracing method, we found that the image of the target on the retina coincides with the area centralis. For that we assumed that the center of the eyecup, which is represented by half a sphere and on which the retina lies, is aligned with the centers of the lens and of the pupil. However, from the front view images of the fish's eye, it can be seen that there is a small translation of the lens center relative to the center of the pupil (see Figure 4C). Hence, we have to take into account that the center of the lens may have vertical and/or horizontal translation (relative to the plane of the water surface) with respect to the center of the eyecup, which consequently may affect our results of finding the location of the image of the target on the retina. To account for this issue, we can consider the worst-case scenario where the lens is translated in the maximal possible amplitude and consider the consequences of this on our measurements. From Figure 4C we can see the centers of the pupil and the lens are in agreement with a translation difference of up to $0.2r$ (where r is the lens radius), while the lens (in the hyperopic case, see Figure 4A) is at the center of the eyecup. Taking a small translation of a few millimeters of the lens from the eyecup center along the water surface plane will result in a similar translation of the target's projection on the retina, since the distance to the target is high (57 cm above the fish) relative to the lens translation. We found that a translation of $0.2r$, for $r = 1.8$ mm (typical for a fish with eye radius of 5 mm that we used) will result in translation of 0.36 mm of the target's image on the retina, which corresponds to 4°, while the radius of the area centralis is 6°. This describes the worst-case scenario of our error in locating the area centralis exact location. Looking at a case of a vertical translation of the lens center with regard to the eyecup center, we expect no effect on the position of the target's image on the retina. In this case, since the fish eyes are beneath the target in a direction perpendicular to the water surface (Figure 2A), an imaginary line can be drawn between the target, the lens center, and the projection of the target on the retina. Thus, a vertical translation of the lens will have no effect on the direction of the target's projection with regard to the eyecup.

Acknowledgments

This work was supported by The Israel Science Foundation grant no. 502/07 and The Human Frontiers Science Program. We would like to thank G. Glusman and R. Marom for technical assistance, and the generous support of the Zlotowski center for neuroscience research, the Frankel Fund, and the Paul Ivanier Robotics Center at Ben-Gurion University.

Commercial relationships: none.
Corresponding author: Ronen Segev.
Email: ronensgv@bgu.ac.il.

Address: Department of Life Sciences and Zlotowski Center for Neuroscience, Ben-Gurion University of the Negev, Beer-Sheva, Israel.

References

Ben-Simon, A., Ben-Shahar, O., & Segev, R. (2009). Measuring and tracking eye movements of a behaving archer fish by real-time stereo vision. *Journal of Neuroscience Methods*, *184*(2), 235–243.

Ben-Simon, A., Ben-Shahar, O., Vasserman, G., & Segev, R. (in press). Predictive saccade in the absence of smooth pursuit: Interception of moving targets in the archer fish. *Journal of Experimental Biology*.

Brainard, D. H. (1997). The psychophysics toolbox. *Spatial Vision*, *10*(4), 433–436.

Charman, W. N., & Tucker, J. (1973). The optical system of the goldfish eye. *Vision Research*, *13*(1), 1–8.

Demer, J. L., Kono, R., & Wright, W. (2003). Magnetic resonance imaging of human extraocular muscles in convergence. *Journal of Neurophysiology*, *89*(4), 2072–2085.

Dill, L. M. (1977). Refraction and the spitting behavior of the archerfish (*Toxotes chatareus*). *Behavioral Ecology and Sociobiology*, *2*(2), 169–184.

Easter, S. S., Jr., Johns, P. R., & Baumann, L. R. (1977). Growth of the adult goldfish eye—I: Optics. *Vision Research*, *17*(3), 469–477.

Hirsch, J., & Curcio, C. A. (1989). The spatial resolution capacity of human foveal retina. *Vision Research*, *29*(9), 1095–1101.

Ikeda, H. (1979). Physiological basis of visual acuity and its development in kittens. *Child Care Health Development*, *5*(6), 375–383.

Kolb, H. (2003). How the retina works. *American Scientist*, *91*(1), 28–35.

Land, M. F. (1999). Motion and vision: Why animals move their eyes. *Journal of Comparative Physiology A: Neuroethology, Sensory, Neural, and Behavioral Physiology*, *185*(4), 341–352.

Land, M. F., & Nilsson, D.-E. (2012). *Animal eyes*. Oxford, UK: Oxford University Press.

Landau, L., & Lifshitz, E. (1982). Mechanics, Vol. I of Course on Theoretical Physics. *Butterworth-Heinemann, 40*, 1050.

Luling, K. (1958). Morphologisch-anatomische und histologische untersuchungen am auge des schutzenfisches toxotes jaculatrix (Pallas, 1766) nebst bemerkungen zum spuckgehahaben. *Zeitschrift für Morphologie und Ökologie der Tiere*, *47*, 529–610.

Luling, K. (1963). Archer fish. *Scientific American*, *209*, 100.

Masland, R. H. (2001). The fundamental plan of the retina. *Nature Neuroscience*, *4*, 877–886.

Mokeichev, A., Segev, R., & Ben-Shahar, O. (2010). Orientation saliency without visual cortex and target selection in archer fish. *Proceedings of the National Academy of Sciences*, *107*(38), 16726–16731.

Neumeyer, C. (2003). Wavelength dependence of visual acuity in goldfish. *Journal of Comparative Physiology A: Neuroethology, Sensory, Neural, and Behavioral Physiology*, *189*(11), 811–821.

Plotkin, A., Paperno, E., Vasserman, G., & Segev, R. (2008). Magnetic tracking of eye motion in small, fast-moving animals. *IEEE Transactions on Magnetics*, *44*(11), 4492–4495.

Rodieck, R. W. (1998). *The first steps in seeing*. Vol. *15*. Sunderland, UK: Sinauer Associates.

Rossel, S., Corlija, J., & Schuster, S. (2002). Predicting three-dimensional target motion: How archer fish determine where to catch their dislodged prey. *Journal of Experimental Biology*, *205*(Pt 21), 3321–3326.

Sadler, J. (1973). The focal length of the fish eye lens and visual acuity. *Vision Research*, *13*(2), 417–423.

Schimidt, J. T., Cicerone, C. M., & Easter, S. S. (1978). Expansion of the half retinal projection to the tectum in goldfish: An electrophysiological and anatomical study. *Journal of Comperative Neurology*, *177*(2), 257–277.

Schlegel, T., & Schuster, S. (2008). Small circuits for large tasks: High-speed decision-making in archerfish. *Science*, *319*(5859), 104–106.

Schuster, S., Rossel, S., Schmidtmann, A., Jäger, I., & Poralla, J. (2004). Archer fish learn to compensate for complex optical distortions to determine the absolute size of their aerial prey. *Current Biology*, *14*(17), 1565–1568.

Segev, R., Puchalla, J., & Berry, M. J., II. (2006). Functional organization of ganglion cells in the salamander retina. *Journal of Neurophysiology*, *95*(4), 2277–2292.

Segev, R., Schneidman, E., Goodhouse, J., & Berry, M. J., II. (2007). Role of eye movements in the retinal code for a size discrimination task. *Journal of Neurophysiology*, *98*(3), 1380–1391.

Somiya, H., & Tamura, T. (1973). Studies on the visual

accommodation in fishes. *Japan Journal of Ichthyology*, *20*, 193–206.

Strenk, S. A., Semmlow, J. L., Strenk, L. M., Munoz, P., Gronlund-Jacob, J., & DeMarco, J. K. (1999). Age-related changes in human ciliary muscle and lens: A magnetic resonance imaging study. *Investigative Ophthalmology & Visual Science*, *40*(6), 1162–1169, http://www.iovs.org/content/40/6/1162 [PubMed] [Article].

Tamura, T., & Wisby, W. J. (1963). The visual sense of pelagic fishes especially the visual axis and accommodation. *Bulletin of Marine Science*, *13*(3), 433–448.

Temple, S., Hart, N. S., Marshall, N. J., & Collin, S. P. (2010). A spitting image: Specializations in archerfish eyes for vision at the interface between air and water. *Proceedings of the Royal Society B: Biological Sciences*, *277*(1694), 2607–2615.

Timmermans, P. (2000). Prey catching in the archer fish: Marksmanship, and endurance of squirting at an aerial target. *Netherlands Journal of Zoology*, *50*(4), 411–423.

Timmermans, P. (2001). Prey catching in the archer fish: Angles and probability of hitting an aerial target. *Behavioral Processes*, *55*(2), 93–105.

Vasserman, G., Shamir, M., Ben Simon, A., & Segev, R. (2010). Coding "what" and "when" in the archer fish retina. *PLoS Computational Biology*, *6*(11), e1000977.

Ventura, T., Manor, R., Aflalo, E. D., Weil, S., Raviv, S., Glazer, L., Sagi, A., et al. (2009). Temporal silencing of an androgenic gland-specific insulin-like gene affecting phenotypical gender differences and spermatogenesis. *Endocrinology*, *150*(3), 1278–1286.

Wohl, S., & Schuster, S. (2006). Hunting archer fish match their take-off speed to distance from the future point of catch. *Journal of Experimental Biology*, *209*(Pt 1), 141–151.

Wohl, S., & Schuster, S. (2007). The predictive start of hunting archer fish: A flexible and precise motor pattern performed with the kinematics of an escape C-start. *Journal of Experimental Biology*, *210*(Pt 2), 311–324.